crystals

MDPI

Article

Local Charge Distribution in Ga_xPd_y Intermetallics: Characterizing Catalyst Surfaces from Large-Scale Molecular Mechanics Simulations

Tanakorn Wonglakhon [1,2,*], Sven Maisel [3], Andreas Görling [3] and Dirk Zahn [2,*]

[1] KOSEN-KMITL, King Mongkut's Institute of Technology Ladkrabang, Bangkok 10520, Thailand
[2] Lehrstuhl für Theoretische Chemie/Computer Chemie Centrum, Friedrich-Alexander Universität Erlangen-Nürnberg, Nägelsbachstraße 25, D-91052 Erlangen, Germany
[3] Lehrstuhl für Theoretische Chemie, Friedrich-Alexander Universität Erlangen-Nürnberg, Egerlandstraße 3, D-91058 Erlangen, Germany; sven.maisel@fau.de (S.M.); andreas.goerling@fau.de (A.G.)
* Correspondence: tanakorn.wo@kmitl.ac.th (T.W.); dirk.zahn@fau.de (D.Z.)

Abstract: We combine the charge equilibration (QEq) method with the modified embedded atom model (MEAM) to describe a series of intermetallic Ga_xPd_y compounds at near DFT accuracy. Apart from structure, energetics and elastic properties, a particular focus is dedicated to the partial charges on Ga and Pd sites in the bulk and on flat/terraced surfaces. By the example of $GaPd_2$, we suggest a computationally very efficient approach to assessing the crystal faces and steps of interesting prospect for catalytic activity. To this end, we suggest enhanced catalytic activity of (010) faces by our simulation models that demonstrate particularly large charge transfer between surface Ga and Pd species, namely +0.8 and −0.4, whereas for the (100) and (001) faces local polarization is less than +0.6 and −0.3, respectively. Moreover, the study of rough surfaces is demonstrated from a small series of 10 nm sized simulation models featuring terraces. Local polarization of the atoms at the steps ranges from +0.5 to +1.1 and −0.5 to −0.3 for the Ga and Pd species, respectively.

Keywords: partial charges; Ga-Pd intermetallic compounds; MEAM potentials; QEq method; catalytic activity

check for updates

Citation: Wonglakhon, T.; Maisel, S.; Görling, A.; Zahn, D. Local Charge Distribution in Ga_xPd_y Intermetallics: Characterizing Catalyst Surfaces from Large-Scale Molecular Mechanics Simulations. *Crystals* **2024**, *14*, 592. https://doi.org/10.3390/cryst14070592

Academic Editor: Xiaochun Li

Received: 10 June 2024
Revised: 21 June 2024
Accepted: 25 June 2024
Published: 27 June 2024

Copyright: © 2024 by the authors. Licensee MDPI, Basel, Switzerland. This article is an open access article distributed under the terms and conditions of the Creative Commons Attribution (CC BY) license (https://creativecommons.org/licenses/by/4.0/).

1. Introduction

Intermetallic compounds of gallium (Ga) and palladium (Pd) have attracted considerable attention in catalysis research due to their potential in promoting various chemical reactions, including the partial hydrogenation of acetylene [1–5], methanol steam reforming [6,7], methanol and dimethyl ether syntheses [8–11], and methanol oxidation [12]. Since the first publication of the Ga-Pd phase diagram [13,14], the diverse intermetallic phases of Ga_xPd_y, particularly $GaPd_2$, has intensified interest in understanding the diverse intermetallic phases of Ga_xPd_y and their catalytic properties [15]. To this end, recent studies by Armbrüster et al. [2,16] highlighted the exceptional selectivity of Ga_7Pd_3, GaPd, and $GaPd_2$ in semi-hydrogenation reactions, surpassing conventional commercial catalysts.

From the viewpoint of atomic simulation, density functional theory (DFT) or quantum chemical calculations may provide valuable insights into the electronic and structural influences on catalytic activity. Notably, investigations into the electronic and structural influences on the catalytic activity of $GaPd_2$ compounds, with Sn substitution on Ga atom as $Ga_{1-x}Sn_xPd_2$ ($0 \leq x \leq 1$), have revealed correlations between pronounced charge transfer from p elements to palladium and catalytic activity variation [17,18]. While informative, these theoretical studies are limited by computational cost and scalability, restricting the size of the models to hundreds of atoms. Thus, characterization of surfaces is limited to nm scale slab models and investigations of surface roughness are seriously hindered by the drastic computational effort needed.

As a cost-effective alternative to DFT, molecular mechanics models featuring the charge equilibration method (QEq) offer near-DFT accuracy in the frame-work of interatomic potentials [19]. For intermetallic Ga-Pd systems, so far embedded atom model (EAM) potentials [20,21] were developed, however not yet incorporating the QEq approach [22]. To clearly discriminate the charge transfer between the two metal species and the metallic bonding in more general terms, we argue that a joint fitting process is needed to obtain a comprehensive combination of QEq and EAM potentials.

This is the aim of the present study from a modelling viewpoint. In turn, from the perspective of applications, we shall take use of the reduced computational costs to outline the study of complex catalyst surfaces and thus pave the road to millions of atoms models.

2. Methods and Models

2.1. DFT Calculations

The DFT Calculations were performed using the Vienna Ab-initio Simulation Package (VASP) [23,24] with the projector augmented wave (PAW) approach [25] employed to represent the atomic cores of Ga and Pd atoms. The Perdew-Burke-Ernzerhof (PBE) exchange correlation functional [26] was utilized, along with a plane wave basis set with a kinetic energy cutoff of 700 eV. Convergence criteria included a tight threshold of 10^{-8} eV for wave functions and a first-order Methfessel-Paxton smearing with a width of 0.2 eV [27].

The structural characterization of solid Ga_xPd_y intermetallic compounds relies on unit cell models and 3D periodic boundary conditions. Structural relaxation was performed until all forces were below 0.001 eV/Å. Γ-including k-point meshes of varying dimensions ($11 \times 7 \times 11$, $8 \times 8 \times 5$, $6 \times 6 \times 6$, $10 \times 10 \times 10$, $9 \times 5 \times 12$, $9 \times 12 \times 6$, $9 \times 12 \times 3$, and $13 \times 13 \times 13$) were used in geometry optimization for Ga, Ga_5Pd, Ga_7Pd_3, GaPd, Ga_3Pd_5, $GaPd_2$, Ga_2Pd_5, and Pd, respectively. Additionally, for the calculation of mechanical properties, the mesh size was doubled. In VASP, the elastic tensor was computed through strain-stress analysis of the equilibrium structure. Six finite distortions were applied, and elastic constants were derived from the resulting strain-stress relationship [28]. Bader atomic charge calculation was utilized to determine the partial charges of Ga and Pd atoms for all systems discussed [29–32].

2.2. EAM and Modified EAM Potentials

The EAM potential is widely used to model metals and alloys due to its ability to account for coordination-dependent binding strength. For Ga-Pd systems, we recently presented an EAM potential for modelling Ga-Pd intermetallic crystals and liquid alloys [22]. Essentially, the EAM is expressed as

$$E = \sum_i F_i(\rho_i) + \frac{1}{2} \sum_{i,j,i \neq j} \phi_{ij}(r_{ij}), \quad (1)$$

$$\rho_i = \sum_{j,j \neq i} f_j(r_{ij}), \quad (2)$$

where $F_i(\rho_i)$ is the energy for embedding an atom i into a site associated with the background electron density ρ_i. This term was derived from the summation of the densities of surrounding neighbors $f_j(r_{ij})$, Equation (2), therefore adding the many-body interaction to the two-body interaction described by $\phi_{ij}(r_{ij})$. Various formulae for the two terms in Equations (1) and (2) have been proposed; our previous EAM potential for the Ga-Pd system is based on the formalism proposed by Mei et al. [33].

Although the EAM potential is sufficient for modelling various metals and alloys, for some materials with covalent bonds, such as silicon and gallium, modification of the EAM potential is needed. For this, Baskes modified the EAM to include angular terms, leading to the modified EAM potential (MEAM). Full details of the MEAM potentials are not repeated here and we instead refer to the references [34–36]. In what follows, only few aspects of the MEAM are discussed in detail to describe the background of the underlying parameters.

For the MEAM potential, the embedding energy $F_i(\rho_i)$ is essentially the same as that in the EAM potential proposed by Baskes [36] and is written as

$$F_i(\rho_i) = AE_c \frac{\rho_i}{\rho^0} \ln\left(\frac{\rho_i}{\rho^0}\right), \tag{3}$$

where A is an adjustable parameter (fitted to DFT), and E_c and ρ_0 are the cohesive energy and the electron density of the reference structure, respectively. The main change to the EAM potential lies in the treatment of the background electron density ρ_i. In the EAM potential ρ_i originates from the superposition of spherical partial electron densities centered on neighboring atoms j (Equation (2)), whereas in the MEAM, this is modified to take an angular term into account by weights originating to the projections of the distances between atoms i and j in x, y, and z directions—see reference [37] for details. The combination of those angular dependent terms reads

$$\Gamma = \sum_{l=1}^{3} t^{(l)} \left(\rho^l / \rho^0\right)^2, \tag{4}$$

where t^l (l = 1,3) are constants fitted to data from DFT calculations. The *atomic* electron densities are used to calculate the angular-dependent partial electron densities and are represented as exponential functions with decay constants $\beta^{(k)}$ (k = 0–3) fitted to DFT calculations. In turn, ρ_i is taken as

$$\rho_i = \rho^0 \sqrt{1+\Gamma}\,. \tag{5}$$

For the pair potential, the same formula as in the modified EAM potential developed by Baskes et al. [35–37], is employed here:

$$\phi_{ij}(r_{ij}) = \frac{2}{Z}\left\{E^u(R) - F\left(\rho^0(R)\right)\right\}, \tag{6}$$

where Z is the number of nearest neighbor atoms of the reference structure, $E^u(R)$ is the energy per atom of the reference structure as a function of nearest neighbor distance R, and $F\left(\rho^0(R)\right)$ has the same definition as that in Equation (1), but refers to the reference structure. The $E^u(R)$ can be calculated either from first-principles calculations or from the universal equation of state by Rose et al. [38] This universal equation of state, which is also used by Baskes et al. [34–36], is written as

$$E^u(r_{ij}) = -E_c\left(1 + a^* + \frac{r_e}{R}\delta {a^*}^3\right)e^{-a^*}, \tag{7}$$

$$a^* = \alpha\left(\frac{R}{r_e} - 1\right), \tag{8}$$

$$\alpha^2 = \frac{9\Omega B}{E_c}, \tag{9}$$

where Ω and B are the equilibrium atomic volume and bulk modulus of the reference structure, respectively, and the δ parameter in Equation (7) is the adjustable parameter used to make the potential more flexible and thus better represent the bulk modulus of the reference material.

In the MEAM potential, the pair potential and the atomic electron density are scaled by the angular screening factor (S_{ik}) as first proposed by Baskes [36] as follows

$$S_{ik} = \prod_{j \neq i,\, k} S_{ijk}, \tag{10}$$

where S_{ijk} describes how an atom k screens the interaction between atoms i and j. This is controlled by the C parameter in the ellipse equation:

$$x^2 + \frac{y^2}{C} = \left(\frac{R_{ik}}{2}\right)^2, \tag{11}$$

$$C = \frac{2\left(X_{ij} + X_{jk}\right) - \left(X_{ij} - X_{jk}\right)^2 - 1}{1 - \left(X_{ij} - X_{jk}\right)^2}, \tag{12}$$

$$X_{ij} = \left(\frac{R_{ij}}{R_{ik}}\right)^2 \text{and } X_{jk} = \left(\frac{R_{jk}}{R_{ik}}\right)^2. \tag{13}$$

By drawing the ellipse on three atoms and imposing the two limiting ellipses via C_{min} *and* C_{max} parameters, the magnitude of screening of the ij interaction can be determined by the positions of the j atoms. If atom j is outside the outer ellipse ($C > C_{max}$), $S_{ijk} = 0$ and the ij interaction is completely unscreened. On the other hand, if atom j is inside the inner ellipse, $S_{ijk} = 1$ and the ij interaction is completely active. In turn, when atom j lies between the inner and outer ellipses, smooth screening is provided via:

$$S_{ijk} = \left[1 - \left(\frac{C_{max} - C}{C_{max} - C_{min}}\right)^4\right]^2. \tag{14}$$

This screening factor also determines if the partial electron density has the contribution from the second-nearest neighbor; by slightly lowering the C_{min} value (which is usually set to a default value of 2), the second-nearest neighbor is considered. The MEAM potential in this study also considers the contribution from the second nearest neighbor. Putting all parts together, in this study, we created the MEAM for the Ga-Pd intermetallic compounds based on the elementary MEAM potentials for Ga developed by Baskes et al. [37] and Pd by Lee et al. [39], but create newly fitted parameters stemming from integrating energy/forces derived from the MEAM and the QEq methods.

2.3. Charge Equilibration Method (QEq)

To allow the modelling of charge transfer and polarization effects in Ga-Pd systems, the charge equilibration method (QEq) is coupled with the EAM and MEAM potentials, respectively. The formulation of total energy according to Equation (1) is thus extended to:

$$E_{total} = \sum_i F_i(\rho_i) + \frac{1}{2}\sum_{i,j,i\neq j} \phi_{ij}(r_{ij}) + \sum_i E_i(Q_i) + \sum_{i\neq j} \frac{Q_i Q_j}{4\pi\varepsilon_0 r_{ij}} \tag{15}$$

where $E_i(Q_i)$ is the energy of atom i as a function of charge Q from the QEq method. Expanding $E_i(Q_i)$ as a Taylor series from the charge-neutral metal atom up to the second order leads to

$$E_i(Q_i) = E_i(0) + Q_i \cdot \left(\frac{\partial E_i}{\partial Q_i}\right)\Big|_0 + \frac{1}{2}Q_i^2 \cdot \left(\frac{\partial^2 E_i}{\partial {Q_i}^2}\right)\Big|_0 \tag{16}$$

Therein, the two derivatives are interpreted as QEq-specific force-field parameters that control the polarizability of the individual atoms i. The most common approach to assessing this data from the ionization potential IP and the electron affinity EA of the single atom, indeed by adding/subtracting $E_i(-1)$ and $E_i(+1)$ we get:

$$\left(\frac{\partial E_i}{\partial Q_i}\right) = \frac{1}{2}(IP + EA) = \chi_i^0 \tag{17}$$

and

$$\left(\frac{\partial^2 E_i}{\partial Q_i^2}\right) = IP - EA = J_{ii}^0 \tag{18}$$

where χ_i^0 and J_{ii}^0 are interpreted as the electronegativity and the "self-Coulomb potential" of the isolated atom i, respectively. The constant J_{ii}^0 equals to the atomic hardness η_i^0 multiplied by 2. By adding the Coulomb interactions to the summation of energies of all atoms, we then obtain the total electrostatic energy of all N atoms as

$$E(Q_1, \ldots, Q_N) = \sum_i \left[E_i(0) + Q_i \cdot \chi_i^0 + \frac{1}{2} Q_i^2 \cdot J_{ii}^0\right] + \sum_{i \neq j} \frac{Q_i Q_j}{4\pi\varepsilon_0 r_{ij}} \tag{19}$$

The derivative of $E(Q_1, \ldots, Q_N)$ with respect to Q_i leads to the electronegativity $\chi_i(Q_i)$ of atom i in the system:

$$\chi_i(Q_i) = \chi_i^0 + Q_i \cdot J_{ii}^0 + \sum_{i \neq j} \frac{Q_i Q_j}{4\pi\varepsilon_0 r_{ij}} \tag{20}$$

Based on Sanderson's principle, the electronegativity of all atoms within the metal particle or bulk crystal will equalize:

$$\chi_1(Q_1) = \chi_2(Q_2) = \ldots = \chi_N(Q_N)\,, \tag{21}$$

with the restriction that the total charge of the system must be conserved.

In what follows, we use two variations of the QEq approach. This involves the most common assessment of χ_i^0 and J_{ii}^0 via Equations (17) and (18), thus using the experimental IP and EA of single Ga and Pd atoms, respectively [40–42]. On this basis, our setup denoted as EAM/QEq$_{exp}$ refers to χ_{Ga}^0 = 3.1490 eV/χ_{Pd}^0 = 4.4481eV and η_{Ga}^0 = 2.84775 eV/η_{Ga}^0 = 3.88600 eV, respectively. Moreover, in a parallel setup denoted as MEAM/QEq$_{exp}$ we perform a joint fitting of the MEAM and the QEq parameters.

2.4. Molecular Mechanics Calculations

The molecular mechanics simulations of the intermetallic bulk crystals were formed with the General Utility Lattice Program (GULP) package [43]. Starting from the experimental crystal structures, full optimization of all atom positions and cell vectors were performed before assessing elastic constants and partial charges. GULP was also used for fitting the MEAM/QEq parameters to best reproduce the DFT reference data. In turn, our molecular mechanics calculations dedicated to intermetallic clusters and surface slab models were performed with the Large-scale Atomic/Molecular Massively Parallel Simulator (LAMMPS) program [44]. In all calculations, we describe the Coulomb interactions via the damped shifted force potential with a real space cut-off distance of 6 Å and a damping parameter of 0.05 Å^{-1}, respectively [45].

3. Results

The embedded atom models readily provide quite accurate interaction potentials for studying bulk metals and alloys. Since the employed three-body functions explicitly consider the coordination of atomic coordination when assigning binding strength, it is also quite common to use EAM and MEAM potentials for modelling metal clusters and crystal faces. To characterize local charges, it appears as an intuitive extension of the EAM/MEAM description to simply add interaction terms stemming from the QEq model to our molecular mechanics description. Upon charge transfer between the atomic species of an alloy such as the Ga_xPd_y compounds investigated here, we must however account for the Coulomb interactions—which are not part of the original fitting of EAM/MEAM parameters.

In what follows, we follow two strategies to account for charge transfer in Ga_xPd_y alloys. Our first setup, denoted as MEAM$_{mix}$/QEq$_{exp}$ reflects the direct combination of MEAM and conventional QEq$_{exp}$ based on second order polynomial (Equation (16)) and

experimental inputs to reproduce ionization energy and electron affinity of isolated Ga and Pd atoms (Equations (17) and (18)). The Ga-Ga and Pd-Pd MEAM parameters were taken from refs. [37,39], respectively, whereas details of mixing the $MEAM_{mix}$ potentials are provided in Table 1. For comparison, the mixed MEAM model is compared to our recently developed EAM model for Ga-Pd interactions as reported in ref. [22]. We pointed out that both of these EAM/MEAM models do not include explicit Coulomb interaction terms. Thus, simply adding QEq_{exp} interactions to the EAM/MEAM potentials alters the structural and mechanical properties of the alloy, possibly leading to lower accuracy as compared to the original (stand-alone EAM or MEAM) parameterization.

Table 1. MEAM and QEq parameters for describing Ga-Pd alloys. The parameters were obtained from (a) conventional mixing rules for $MEAM_{mix}$ and conventional QEq_{exp} parameterization based on single atom ionization energy and electron affinity from the experiment (refs. [40–42], respectively, see also Equations (17) and (18)). Moreover, (b) we present a newly created $MEAM_{new}/QEq_{new}$ model as obtained from fitting all interaction parameters.

Ga-Pd i−j	**Mixing MEAM and Qeq ($MEAM_{mix}/QEq_{exp}$)**		**Newly Fitted $MEAM_{new}/QEq_{new}$**
	Parameters	**Source of Parameter**	
E_c/eV	3.782	DFT calc.	4.328305
r_e/Å	2.693	DFT calc.	2.612755
α	5.424	0.5 ($\alpha^{Ga} + \alpha^{Pd}$)	5.472011
δ	0.0735	0.5 ($\delta^{Ga} + \delta^{Pd}$)	0.012891
$C_{min}(i-i-j)$	1.545	0.5 [$C_{min}(i-i-i)$ $+C_{min}(j-j-j)$]	0.440
$C_{min}(j-j-i)$	1.545		1.100
$C_{min}(i-j-i)$	1.545		1.545
$C_{min}(j-i-j)$	1.545		1.545
$C_{max}(i-i-j)$	2.8	0.5 [$C_{max}(i-i-i)$ $+C_{max}(j-j-j)$]	2.7
$C_{max}(j-j-i)$	2.8		2.8
$C_{max}(i-j-i)$	2.8		2.8
$C_{max}(j-i-j)$	2.8		2.8
ρ_0^{Ga}/ρ_0^{Pd}	1.0	ρ_0 of Ga and Pd	1.0
χ_{Ga}/eV	3.1490	EA, IE from exp.	2.382024
η_{Ga}/eV	2.84775	EA, IE from exp.	0.555958
χ_{Pd}/eV	4.4481	EA, IE from exp.	4.055200
η_{Pd}/eV	3.88600	EA, IE from exp.	2.637226

In turn, our second setup is based on newly parameterized $MEAM_{new}$ and QEq_{new} interaction potentials. For this, all of the involved parameters (Table 1) were optimized in a joint fitting procedure. In full analogy to our earlier study reported in ref. [22] we use $GaPd_2$ crystals (space group Pnma, no. 62) as reference (in terms of structure, lattice energy and elastic properties). The resulting $MEAM_{new}$ and QEq_{new} parameters are shown in Table 1, whereas a comparison of the structural and elastic properties used as benchmarks to fitting the new potentials is provided in Table 2.

Comparing the two types of tailor-made Ga-Pd potentials, namely the EAM model from our previous work and the newly created $MEAM_{new}/QEq_{new}$ model we clearly find improved reproduction of the structural data and mechanical properties of $GaPd_2$ as used for parameterization. However, considering the additional set of tunable parameters, this finding is quite unsurprising. More rigorous benchmarking is obtained by contrasting the results for the series of Ga_xPd_y crystals presented in Tables 3 and 4. In Table 3, we listed the unit cell constants as observed from experiment, DFT calculations, conventional EAM or MEAM modelling in absence of charge polarization and with the account of charge transfer

between the alloy components from QEq. Likewise, the same series of interaction models is benchmarked in terms of the lattice energy in Table 4.

Table 2. Structural data and mechanical properties of $GaPd_2$ (space group Pnma, no. 62) as used for fitting the Ga-Pd interactions in our previous EAM potential [22] and the present $MEAM_{new}/QEq_{new}$ potential. Bulk and shear moduli are calculated from the Hill approximation [46], respectively.

Experiment [47]		**Ab-Initio Reference [22]**	**EAM [22]**	**$MEAM_{new}/QEq_{new}$**
a/Å	5.4829	5.4816	5.4072	5.3485
b/Å	4.0560	4.0545	4.1437	4.0693
c/Å	7.7863	7.8080	7.8601	7.8585
Elastic constants/10 GPa				
c_{11}		27.62	22.562	26.244
c_{12}		13.765	15.703	14.805
c_{13}		13.906	14.248	13.844
c_{22}		24.992	22.421	27.395
c_{23}		14.849	16.815	16.656
c_{33}		26.876	24.107	27.194
c_{44}		6.551	3.641	6.563
c_{55}		4.035	2.268	3.374
c_{66}		7.447	3.924	5.290
B		17.869	18.040	19.012
G		5.931	3.354	5.255

Table 3. Comparison of structural parameters (Å) of Ga_xPd_y crystals as obtained from the experiment, DFT, EAM, EAM/QEq_{exp}, $MEAM_{mix}$, $MEAM_{mix}/QEq_{exp}$, and $MEAM_{new}/QEq_{new}$ potentials, respectively. As error margins, the percentage of the deviation from the experimental values is shown in square brackets.

		Exp.	**DFT [22]**	**EAM [22]**	**EAM/ QEq_{exp}**	**$MEAM_{mix}$**	**$MEAM_{mix}$ /QEq_{exp}**	**$MEAM_{new}$/ QEq_{new}**
Ga_5Pd [13]	a	6.448	6.507 [0.9%]	6.609 [2.5%]	6.382 [1.0%]	6.297 [2.3%]	6.296 [2.4%]	6.213 [3.6%]
	b	6.448	6.507 [0.9%]	6.609 [2.5%]	6.382 [1.0%]	6.297 [2.3%]	6.296 [2.4%]	6.213 [3.6%]
	c	10.003	10.104 [1.0%]	10.253 [2.5%]	10.901 [9.0%]	10.567 [5.6%]	10.565 [5.6%]	10.580 [5.8%]
Ga_7Pd_3 [16]	a	8.772	8.865 [1.1%]	8.935 [1.9%]	8.938 [1.9%]	7.120 [18.8%]	7.135 [18.7%]	8.770 [0.0%]
GaPd [48]	a	4.8969	4.952 [1.1%]	4.9451 [1.0%]	4.9620 [1.3%]	5.052 [3.2%]	5.046 [3.0%]	4.928 [0.6%]
Ga_3Pd_5 [13]	a	5.42	5.514 [1.7%]	5.46 [0.7%]	5.42 [0.0%]	5.572 [2.8%]	5.558 [2.5%]	5.413 [0.1%]
	b	10.51	10.679 [1.6%]	10.59 [0.8%]	10.45 [0.6%]	11.103 [5.6%]	11.067 [5.3%]	10.445 [0.6%]

Table 3. *Cont.*

		Exp.	DFT [22]	EAM [22]	EAM/ QEq_{exp}	$MEAM_{mix}$	$MEAM_{mix}$ /QEq_{exp}	$MEAM_{new}$/ QEq_{new}
	c	4.03	4.064 [0.8%]	4.06 [0.7%]	4.16 [3.2%]	4.047 [0.4%]	4.064 [0.8%]	4.110 [2.0%]
$GaPd_2$ [47]	a	5.4829	5.572 [1.6%]	5.4072 [1.4%]	5.4094 [1.3%]	5.580 [1.8%]	5.570 [1.6%]	5.348 [2.5%]
	b	4.0560	4.092 [0.9%]	4.1437 [2.2%]	4.1411 [2.1%]	4.010 [1.1%]	4.020 [0.9%]	4.069 [0.3%]
	c	7.7863	7.865 [1.0%]	7.8601 [0.9%]	7.8553 [0.9%]	8.317 [6.8%]	8.303 [6.6%]	7.858 [0.9%]
Ga_2Pd_5 [14]	a	5.485	5.507 [0.4%]	5.475 [0.2%]	5.416 [1.3%]	5.572 [1.6%]	5.565 [1.5%]	5.399 [1.6%]
	b	4.083	4.111 [0.7%]	4.075 [0.2%]	4.094 [0.3%]	3.967 [2.8%]	3.973 [2.7%]	3.961 [3.0%]
	c	18.369	18.608 [1.3%]	18.334 [0.2%]	18.477 [0.6%]	19.474 [6.0%]	19.450 [5.9%]	18.787 [2.3%]

Table 4. Comparison of lattice energies (eV/unit cell) of Ga_xPd_y crystals calculated from DFT, EAM, EAM/QEq_{exp}, $MEAM_{mix}$, $MEAM_{mix}$/QEq_{exp}, and $MEAM_{new}$/QEq_{new} methods. As error margins, the percentage of the deviation from the DFT values is shown in square brackets.

	DFT	EAM	EAM/QEq_{exp}	$MEAM_{mix}$	$MEAM_{mix}$ /QEq_{exp}	$MEAM_{new}$/ QEq_{new}
Ga_5Pd	−85.55	−81.03 [4.5%]	−81.85 [3.7%]	−77.88 [7.7%]	−78.69 [6.9%]	−85.87 [0.3%]
Ga_7Pd_3	−162.75	−147.22 [15.5%]	−149.61 [13.1%]	−134.05 [28.7%]	−136.36 [26.4%]	−163.22 [0.5%]
GaPd	−37.97	−34.10 [3.9%]	−34.76 [3.2%]	−29.65 [8.3%]	−30.29 [7.7%]	−38.21 [0.2%]
Ga_3Pd_5	−80.08	−70.63 [9.5%]	−71.98 [8.1%]	−62.00 [18.1%]	−63.22 [16.9%]	−81.62 [1.5%]
$GaPd_2$	−61.26	−53.20 [8.1%]	−54.16 [7.1%]	−46.87 [14.4%]	−47.76 [13.5%]	−62.52 [1.3%]
Ga_2Pd_5	−143.90	−123.29 [20.6%]	−125.32 [18.6%]	−110.13 [33.8%]	−112.05 [31.9%]	−146.15 [2.3%]

Our previous EAM-based model appears quite robust in terms of the observed structures, indeed showing agreement within 3% to the experiment. While the new $MEAM_{new}$/QEq_{new} interaction potential is slightly less accurate in terms of unit cell dimensions, we find drastically better reproduction of the lattice energy and (to more moderate extend) the elastic properties as compared to the DFT reference calculations. Indeed, all of the investigated models show deviations in the ballpark of 10–30% whereas the $MEAM_{new}$/QEq_{new} offers the assessment of cohesive energies at <2.5% precision (Table 4). Likewise, we found the elastic moduli c_{ij} (i,j = 1–6) of $GaPd_2$ within up to 50% error margins for the EAM model, whereas the $MEAM_{new}$/QEq_{new} method leads to <10% deviation from the DFT results.

We point out that the molecular mechanics models based on EAM or MEAM without QEq do consider alloying effects in an implicit manner, and thus already offer reasonable accuracy for modelling processes like mechanical deformation etc. However, when investigating Ga_xPd_y compounds from the perspective of catalysis, it is of particular interest to monitor the local charge distribution in the alloys. For the bulk crystals, this can be accomplished by means of DFT calculations and Bader analysis for assigning local electron

density to atomic sites. In Table 5, we show the partial charges observed in a series of Ga_xPd_y crystals to compare the DFT-based reference with the QEq charges as obtained from the EAM/QEq_{exp}, $MEAM_{mix}$/QEq_{exp} and $MEAM_{new}$/QEq_{new} methods. We find that the local charges predicted by the $MEAM_{new}$/QEq_{new} approach best reproduce the Bader charges as obtained from the DFT reference. This particularly holds for the $GaPd_2$ structure which is investigated for surface effects in the following.

Table 5. Comparison of the partial charges of Ga and Pd atoms in Ga_xPd_y crystals as calculated with DFT, EAM/QEq_{exp}, $MEAM_{mix}$/QEq_{exp}, and $MEAM_{new}$/QEq_{new} methods. The numbers shown in parentheses refer to the total charge of all Ga and Pd species of the corresponding unit cell, respectively.

Crystal	DFT (Bader Charge)		EAM/QEq_{exp}		$MEAM_{mix}$/QEq_{exp}		$MEAM_{new}$/QEq_{new}	
	Ga	Pd	Ga	Pd	Ga	Pd	Ga	Pd
Ga_5Pd	0.12 × 3, 0.15 × 10, 0.18 × 3, 0.23 × 4 **(3.32)**	−0.83 × 4 **(−3.32)**	0.0308 × 4, 0.0315 × 16 **(0.63)**	−0.157 × 4 **(−0.63)**	0.0313 × 4, 0.0314 × 16 **(0.63)**	−0.157 × 4 **(−0.63)**	0.063 × 4, 0.070 × 16, **(1.37)**	−0.343 × 4 **(−1.37)**
Ga_7Pd_3	0.29 × 6, 0.30 × 10, 0.44 × 12 **(10.02)**	−0.82 × 6, −0.85 × 6 **(−10.02)**	0.060 × 16, 0.059 × 12 **(1.67)**	−0.139 × 12 **(−1.67)**	0.0608 × 4, 0.0582 × 8, 0.0593 × 16 **(1.66)**	−0.137 × 4, −0.139 × 8 **(−1.66)**	0.1501 × 4, 0.1557 × 8, 0.1413 × 16 **(4.11)**	−0.341 × 4, −0.343 × 8 **(−4.11)**
GaPd	0.50 × 4 **(2.00)**	−0.50 × 4 **(−2.00)**	0.11 × 4 **(0.44)**	−0.11 × 4 **(−0.44)**	0.11 × 4 **(0.44)**	−0.11 × 4 **(−0.44)**	0.33 × 4 **(1.32)**	−0.33 × 4 **(−1.32)**
Ga_3Pd_5	0.58 × 2, 0.59 × 4 **(3.52)**	−0.33 × 4, −0.34 × 2, −0.38 × 4 **(−3.52)**	0.139 × 4, 0.138 × 2 **(0.83)**	−0.084 × 6, −0.028 × 4 **(−0.83)**	0.1383 × 4, 0.1356 × 2 **(0.82)**	−0.0829 × 2 −0.0831 × 4, −0.0815 × 4, **(−0.82)**	0.51 × 4, 0.52 × 2 **(3.08)**	−0.307 × 2, −0.312 × 2, −0.311 × 2, −0.304 × 4, **(−3.08)**
$GaPd_2$	0.61 × 4 **(2.44)**	−0.28 × 4, −0.33 × 4 **(−2.44)**	0.15 × 4 **(0.60)**	−0.07 × 4, −0.08 × 4 **(−0.60)**	0.15 × 4 **(0.60)**	−0.0743 × 4, −0.0744 × 4 **(−0.60)**	0.60 × 4 **(2.40)**	−0.301 × 2, −0.302 × 2, −0.297 × 2, −0.298 × 2 **(−2.40)**
Ga_2Pd_5	0.63 × 4, 0.65 × 4 **(5.12)**	−0.22 × 4, −0.23 × 4, −0.26 × 4, −0.27 × 4, −0.30 × 4 **(−5.12)**	0.162 × 4, 0.165 × 4 **(1.31)**	−0.066 × 4, −0.063 × 4, −0.065 × 8, −0.068 × 4 **(−1.31)**	0.158 × 4, 0.165 × 4 **(1.29)**	−0.066 × 4, −0.062 × 4, −0.065 × 4, −0.067 × 4, −0.063 × 4 **(−1.29)**	0.658 × 4, 0.745 × 4 **(5.61)**	−0.286 × 4, −0.269 × 4, −0.278 × 4, −0.295 × 4, −0.275 × 4 **(−5.61)**

To one side the improvement achieved by our $MEAM_{new}$/QEq_{new} model appears particularly useful for the investigation of physical vapor deposition processes. To the other, a somewhat related topic is the characterization of rough surfaces, featuring island, plateaus or kinks. Surface reorganization upon such imperfections clearly benefits from interaction models that provide reliable cohesive energy—in terms of both structure and energy. However, with the help of the QEq method, we can now also characterize the distribution of local charges. The $MEAM_{new}$/QEq_{new} not only reasonably reproduces the DFT-Bader charges of the bulk crystal, but also offers the required computational efficiency to assess large scale slab models featuring rough surface landscapes—thus offering more sophisticated structure models to help accounting for "real catalyst" surfaces.

This is illustrated in Figure 1 for a small series of "rough surface" models, namely the (010) face of $GaPd_2$ featuring (a) steps, (b) single ad-atom islands and (c) holes resulting from removing single atoms from the ideal surface. The main driving force for charge transfer in the alloy is the difference in electronegativity of Ga and Pd. However, at surface sites we find individual electrostatic environment according to the local coordination by nearby atoms. Indeed, on the terrace model (Figure 1a), we find that Pd atoms on the plateau surface show −0.32 to −0.37 charge, whereas the steps feature −0.35 to −0.38 charge at the linear edge and −0.33 to −0.42 near kinks (k1,k2,k3). Likewise, the exposed

Pd ad-atoms (Figure 1b) shows different charging subject to local coordination, namely −0.40 for $GaPd_3$ cluster-type arrangements as compared to −0.31 for Ga_2Pd_2 type motifs, respectively. Regarding holes in the (010) surface, (Figure 1c), Pd atoms next to a Ga vacancy (h1) and Pd vacancy (h3) show particularly negative charge up to −0.42.

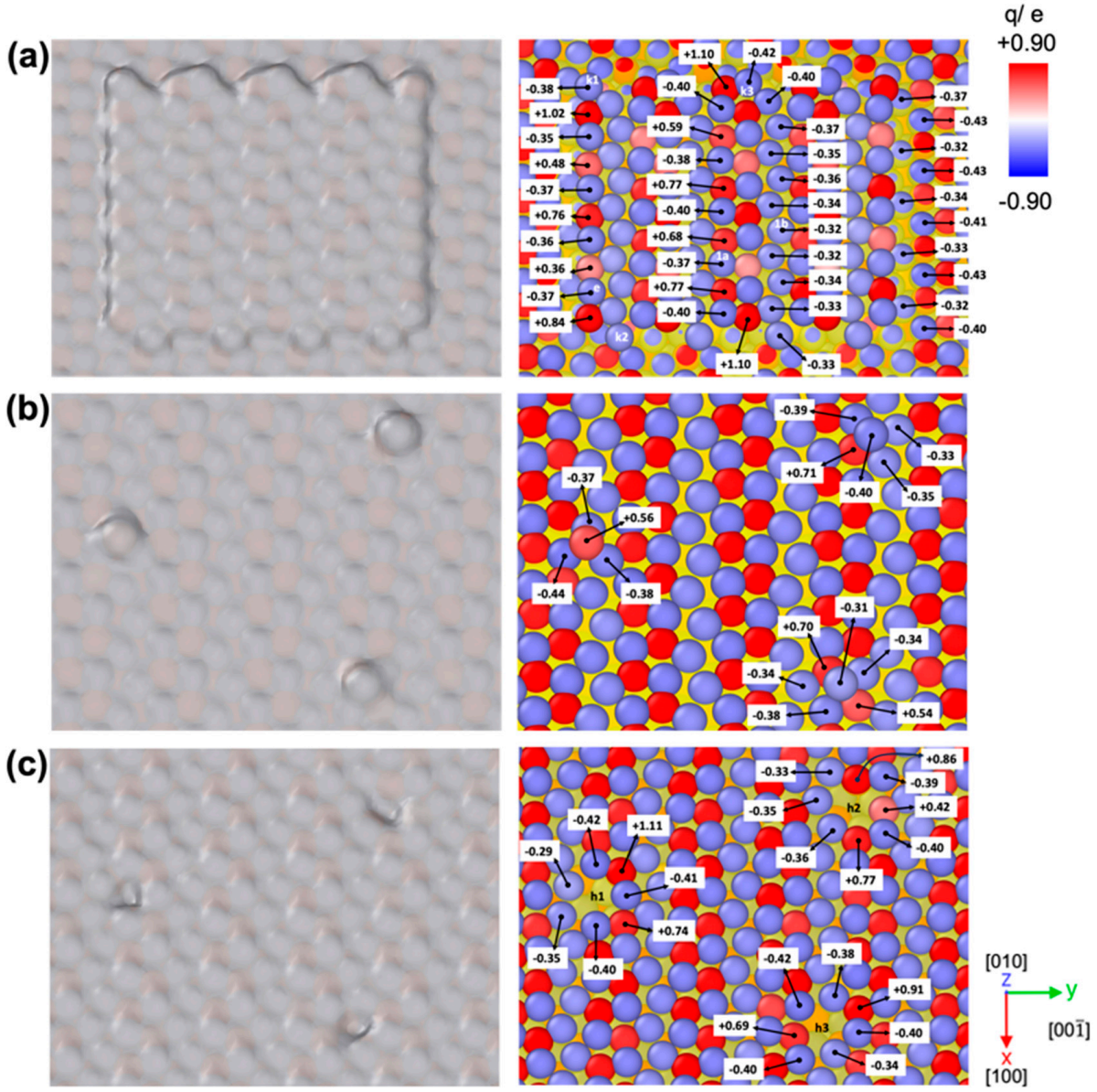


Figure 1. Local charge distributions of Ga and Pd atoms in different regions of rough $GaPd_2$ (010) surface models. Panels (**a**–**c**) refer to a terrace model, adatoms and holes, respectively. The left side of each panel shows surface meshes outlining these areas, while the right side highlights atomic charge via a color code. The charge transfer stems from the difference in electronegativity of the Ga/Pd atomics and the local Coulomb interactions. On this basis, the negative (blue color) charge of Pd atoms show significant variation, namely from −0.29 to −0.44, upon local coordination at edges, island or holes, respectively.

We argue that the charges of Ga and Pd atoms on the different $GaPd_2$ surfaces are of paramount importance for adsorption and activation processes, such as the partial hydrogenation of acetylene. To this end, the extend of charge transfer stemming from the combination of alloying and surface effects at the individual catalyst sites is suggested as indicators for electron donating/withdrawing effects.

To further elaborate this field of application for the $MEAM_{new}/QEq_{new}$ potential, we also investigated the (001), (010), and (100) faces of $GaPd_2$. In particular for semi-hydrogenation, this compound was demonstrated to provide excellent catalytic activity from the experiments of Armbrüster and co-workers [1,16]. Based on the $MEAM_{new}/QEq_{new}$ potential, we calculated specific surface energies for the (001), (010), and (100) faces as 5.09, 1.39, and 3.73 J/m^2, respectively. This indicates that the (010) face exhibits the highest stability, consistent with experimental findings [47]. Moreover, the surface energy of the (010) face was also explored from DFT calculations [49], leading to an ab-initio-based reference value of 1.31 J/m^2—which we find nicely reproduced by the $MEAM_{new}/QEq_{new}$ potential.

The underlying $GaPd_2$ slabs were chosen generously large to ensure bulk behavior in the center (see Table 5 for atomic charges), whilst the surface effects are monitored in terms of the charge transfer between surface atoms as illustrated in Figure 2. In average, we find electron transfer to surface Pd atoms strongest for the (010) face of $GaPd_2$. This suggests that the catalyst performance of the (010) face for semi-hydrogenation reaction may outperform the (100) and (001) faces. This inference is supported by the observed enhancement in electron transfer, which correlates with improved catalytic activity [17,18].

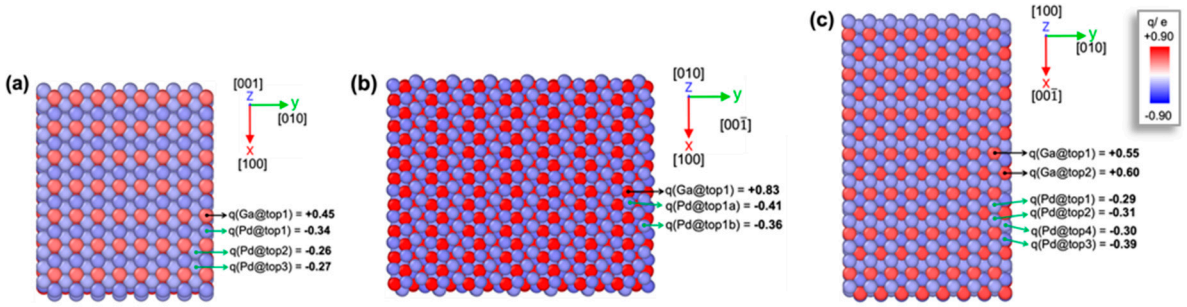


Figure 2. Comparison of $GaPd_2$ slabs featuring (**a**) (001), (**b**) (010), and (**c**) (100) faces. Atomic charges as calculated from the $MEAM_{new}/QEq_{new}$ model are illustrated by a color code. Atom notations include top1, top2, top3, and top4 for the topmost, second top, third top, and fourth top layers, respectively, while top1a and top1b denote atoms at the same topmost layer but different lateral positions.

4. Conclusions

Our study underlines the importance of a systematic approach in developing accurate models for atomic charges in alloys. The original QEq approach based on parameters fitted to reproduce single-atom electron affinity and ionization energy is surely suited for metal and metal alloy clusters, but needs careful confirmation when investigating bulk crystals or surfaces thereof. Indeed, the reasonable performance of common EAM and MEAM potentials in absence of QEq stems from the implicit modelling of charge transfers within the hetero-terms of the atom-atom potentials. To that end, we recently fitted a new EAM potential for Ga-Pd interactions to better describe the mechanical properties of intermetallic Ga_xPd_y compounds. In turn, when employing QEq as explicit term, we suggest to fully re-parameterize both, the QEq and the EAM/MEAM potentials.

On this basis, we demonstrated the characterization of the catalyst $GaPd_2$ at near DFT accuracy. The computational efficiency of our $MEAM_{new}/QEq_{new}$ model outperforms DFT calculations by several orders of magnitude (subject to the choice of the basis set). Our approach therefore offers a new perspective into exploring complex alloy systems, such as extended crystallites, slab models or rough surfaces—as demonstrated by the case studies presented in this work. Moreover, QEq offers an appealing perspective in the direction of electro-catalysis as the implementation of net surfaces as a function of voltage is readily available. Likewise, our models offer the investigation of substrate-induced polarization of nanoparticles and Ga-Pd based liquid alloy droplets—as recently demonstrated for SCALMS (Supported Catalytically Active Liquid Metal Solutions) systems [50].

Author Contributions: Conceptualization, T.W. and D.Z; methodology, T.W., S.M., A.G. and D.Z.; investigation, T.W. and S.M.; writing, T.W., A.G. and D.Z.; All authors have read and agreed to the published version of the manuscript.

Funding: This work was funded by the Deutsche Forschungsgemeinschaft (DFG, German Research Foundation) – Project-ID 431791331 – SFB 1452.

Data Availability Statement: All data can be made available upon request to the authors

Conflicts of Interest: The authors declare no conflicts of interest.

References

1. Ota, A.; Armbrüster, M.; Behrens, M.; Rosenthal, D.; Friedrich, M.; Kasatkin, I.; Girgsdies, F.; Zhang, W.; Wagner, R.; Schlögl, R. Intermetallic Compound Pd_2Ga as a Selective Catalyst for the Semi-Hydrogenation of Acetylene: From Model to High Performance Systems. *J. Phys. Chem. C* **2011**, *115*, 1368–1374. [CrossRef]
2. Armbrüster, M.; Behrens, M.; Cinquini, F.; Föttinger, K.; Grin, Y.; Haghofer, A.; Klötzer, B.; Knop-Gericke, A.; Lorenz, H.; Ota, A.; et al. How to Control the Selectivity of Palladium-Based Catalysts in Hydrogenation Reactions: The Role of Subsurface Chemistry. *ChemCatChem* **2012**, *4*, 1048–1063. [CrossRef]
3. Bauer, M.; Schoch, R.; Shao, L.; Zhang, B.; Knop-Gericke, A.; Willinger, M.; Schlögl, R.; Teschner, D. Structure-Activity Studies on Highly Active Palladium Hydrogenation Catalysts by X-Ray Absorption Spectroscopy. *J. Phys. Chem. C* **2012**, *116*, 22375–22385. [CrossRef]
4. Zimmermann, R.R.; Hahn, T.; Reschetilowski, W.; Armbrüster, M. Kinetic Parameters for the Selective Hydrogenation of Acetylene on $GaPd_2$ and GaPd. *ChemPhysChem* **2017**, *18*, 2517–2525. [CrossRef] [PubMed]
5. Glyzdova, D.V.; Smirnova, N.S.; Leont'eva, N.N.; Gerasimov, E.Y.; Prosvirin, I.P.; Vershinin, V.I.; Shlyapin, D.A.; Tsyrul'nikov, P.G. Synthesis and Characterization of Sibunit-Supported Pd–Ga, Pd–Zn, and Pd–Ag Catalysts for Liquid-Phase Acetylene Hydrogenation. *Kinet. Catal.* **2017**, *58*, 140–146. [CrossRef]
6. Mayr, L.; Lorenz, H.; Armbrüster, M.; Villaseca, S.A.; Luo, Y.; Cardoso, R.; Burkhardt, U.; Zemlyanov, D.; Haevecker, M.; Blume, R.; et al. The Catalytic Properties of Thin Film Pd-Rich $GaPd_2$ in Methanol Steam Reforming. *J. Catal.* **2014**, *309*, 231–240. [CrossRef]
7. Rameshan, C.; Lorenz, H.; Armbrüster, M.; Kasatkin, I.; Klötzer, B.; Götsch, T.; Ploner, K.; Penner, S. Impregnated and Co-Precipitated Pd–Ga_2O_3, Pd–In_2O_3 and Pd–Ga_2O_3–In_2O_3 Catalysts: Influence of the Microstructure on the CO_2 Selectivity in Methanol Steam Reforming. *Catal. Lett.* **2018**, *148*, 3062–3071. [CrossRef]
8. Li, L.; Zhang, B.; Kunkes, E.; Föttinger, K.; Armbrüster, M.; Su, D.S.; Wei, W.; Schlögl, R.; Behrens, M. Ga-Pd/Ga_2O_3 Catalysts: The Role of Gallia Polymorphs, Intermetallic Compounds, and Pretreatment Conditions on Selectivity and Stability in Different Reactions. *ChemCatChem* **2012**, *4*, 1764–1775. [CrossRef]
9. Fiordaliso, E.M.; Sharafutdinov, I.; Carvalho, H.W.P.; Kehres, J.; Grunwaldt, J.D.; Chorkendorff, I.; Damsgaard, C.D. Evolution of Intermetallic $GaPd_2/SiO_2$ Catalyst and Optimization for Methanol Synthesis at Ambient Pressure. *Sci. Technol. Adv. Mater.* **2019**, *20*, 521–531. [CrossRef]
10. García-Trenco, A.; White, E.R.; Regoutz, A.; Payne, D.J.; Shaffer, M.S.P.; Williams, C.K. Pd_2Ga-Based Colloids as Highly Active Catalysts for the Hydrogenation of CO_2 to Methanol. *ACS Catal.* **2017**, *7*, 1186–1196. [CrossRef]
11. Oyola-Rivera, O.; Baltanás, M.A.; Cardona-Martínez, N. CO_2 Hydrogenation to Methanol and Dimethyl Ether by Pd–Pd_2Ga Catalysts Supported over Ga_2O_3 Polymorphs. *J. CO2 Util.* **2015**, *9*, 8–15. [CrossRef]
12. Zerdoumi, R.; Matselko, O.; Rößner, L.; Sarkar, B.; Grin, Y.; Armbrüster, M. Disentangling Electronic and Geometric Effects in Electrocatalysis through Substitution in Isostructural Intermetallic Compounds. *J. Am. Chem. Soc.* **2022**, *144*, 8379–8388. [CrossRef] [PubMed]
13. Schubert, K.; Lukas, H.; Meißner, H.; Bhan, S. Zum Aufbau Der Systeme Kobalt-Gallium, Palladium-Gallium, Palladium-Zinn Und Verwandter Legierungen. *Int. J. Mater. Res.* **1959**, *50*, 534–540. [CrossRef]
14. Khalaff, K.; Schubert, K. Kristallstruktur von Pd_5Ga_2. *J. Less-Common Met.* **1974**, *37*, 129–140. [CrossRef]
15. Armbrüster, M. Intermetallic Compounds in Catalysis–a Versatile Class of Materials Meets Interesting Challenges. *Sci. Technol. Adv. Mater.* **2020**, *21*, 303–322. [CrossRef]
16. Armbrüster, M.; Kovnir, K.; Behrens, M.; Teschner, D.; Grin, Y.; Schlögl, R. Pd-Ga Intermetallic Compounds as Highly Selective Semihydrogenation Catalysts. *J. Am. Chem. Soc.* **2010**, *132*, 14745–14747. [CrossRef]
17. Matselko, O.; Zimmermann, R.R.; Ormeci, A.; Burkhardt, U.; Gladyshevskii, R.; Grin, Y.; Armbrüster, M. Revealing Electronic Influences in the Semihydrogenation of Acetylene. *J. Phys. Chem. C* **2018**, *122*, 21891–21896. [CrossRef]
18. Ormeci, A.; Gaudry, E.; Armbrüster, M.; Grin, Y. Chemical Bonding in the Catalytic Platform Material $Ga_{1-x}Sn_xPd_2$. *ChemistryOpen* **2022**, *11*, e202200185. [CrossRef]
19. Ongari, D.; Boyd, P.G.; Kadioglu, O.; MacE, A.K.; Keskin, S.; Smit, B. Evaluating Charge Equilibration Methods to Generate Electrostatic Fields in Nanoporous Materials. *J. Chem. Theory Comput.* **2019**, *15*, 382–401. [CrossRef]
20. Daw, M.S.; Baskes, M.I. Semiempirical, Quantum Mechanical Calculation of Hydrogen Embrittlement in Metals. *Phys. Rev. Lett.* **1983**, *50*, 1285. [CrossRef]

21. Daw, M.S.; Baskes, M.I. Embedded-Atom Method: Derivation and Application to Impurities, Surfaces, and Other Defects in Metals. *Phys. Rev. B* **1984**, *29*, 6443–6453. [CrossRef]
22. Wonglakhon, T.; Maisel, S.; Görling, A.; Zahn, D. An Embedded Atom Model for Ga-Pd Systems: From Intermetallic Crystals to Liquid Alloys. *J. Chem. Phys.* **2021**, *154*, 014109. [CrossRef] [PubMed]
23. Kresse, G.; Furthmüller, J. Efficiency of Ab-Initio Total Energy Calculations for Metals and Semiconductors Using a Plane-Wave Basis Set. *Comput. Mater. Sci.* **1996**, *6*, 15–50. [CrossRef]
24. Kresse, G.; Furthmüller, J. Efficient Iterative Schemes for Ab Initio Total-Energy Calculations Using a Plane-Wave Basis Set. *Phys. Rev. B* **1996**, *54*, 11169–11186. [CrossRef] [PubMed]
25. Kresse, G.; Joubert, D. From Ultrasoft Pseudopotentials to the Projector Augmented-Wave Method. *Phys. Rev. B* **1999**, *59*, 1758–1775. [CrossRef]
26. Perdew, J.P.; Burke, K.; Ernzerhof, M. Generalized Gradient Approximation Made Simple. *Phys. Rev. Lett.* **1996**, *77*, 3865–3868. [CrossRef]
27. Methfessel, M.; Paxton, A.T. High-Precision Sampling for Brillouin-Zone Integration in Metals. *Phys. Rev. B* **1989**, *40*, 3616–3621. [CrossRef] [PubMed]
28. Le Page, Y.; Saxe, P. Symmetry-General Least-Squares Extraction of Elastic Data for Strained Materials from Ab Initio Calculations of Stress. *Phys. Rev. B* **2002**, *65*, 104104. [CrossRef]
29. Bader, R.F.W. Atoms in Molecules. *Acc. Chem. Res.* **1985**, *18*, 9–15. [CrossRef]
30. Henkelman, G.; Arnaldsson, A.; Jónsson, H. A Fast and Robust Algorithm for Bader Decomposition of Charge Density. *Comput. Mater. Sci.* **2006**, *36*, 354–360. [CrossRef]
31. Sanville, E.; Kenny, S.D.; Smith, R.; Henkelman, G. Improved Grid-Based Algorithm for Bader Charge Allocation. *J. Comput. Chem.* **2007**, *28*, 899–908. [CrossRef] [PubMed]
32. Tang, W.; Sanville, E.; Henkelman, G. A Grid-Based Bader Analysis Algorithm without Lattice Bias. *J. Phys. Condens. Matter* **2009**, *21*, 084204. [CrossRef] [PubMed]
33. Mei, J.; Davenport, J.W.; Fernando, G.W. Analytic Embedded-Atom Potentials for FCC Metals: Application to Liquid and Solid Copper. *Phys. Rev. B* **1991**, *43*, 4653–4658. [CrossRef] [PubMed]
34. Baskes, M.I. Application of the Embedded-Atom Method to Covalent Materials: A Semiempirical Potential for Silicon. *Phys. Rev. Lett.* **1987**, *59*, 2666. [CrossRef] [PubMed]
35. Baskes, M.I.; Nelson, J.S.; Wright, A.F. Semiempirical Modified Embedded-Atom Potentials for Silicon and Germanium. *Phys. Rev. B* **1989**, *40*, 6085. [CrossRef] [PubMed]
36. Baskes, M.I. Modified Embedded-Atom Potentials for Cubic Materials and Impurities. *Phys. Rev. B* **1992**, *46*, 2727–2742. [CrossRef] [PubMed]
37. Baskes, M.I.; Chen, S.P.; Cherne, F.J. Atomistic Model of Gallium. *Phys. Rev. B* **2002**, *66*, 104107. [CrossRef]
38. Rose, J.H.; Smith, J.R.; Guinea, F.; Ferrante, J. Universal Features of the Equation of State of Metals. *Phys. Rev. B* **1984**, *29*, 2963–2969. [CrossRef]
39. Lee, B.-J.; Shim, J.-H.; Baskes, M.I. Semiempirical Atomic Potentials for the Fcc Metals Cu, Ag, Au, Ni, Pd, Pt, Al, and Pb Based on First and Second Nearest-Neighbor Modified Embedded Atom Method. *Phys. Rev. B* **2003**, *68*, 144112. [CrossRef]
40. Kramida, A.; Ralchenko, Y.; Reader, J. *NIST ASD Team NIST Atomic Spectra Database (Version 5.11)*; National Institute of Standards and Technology: Gaithersburg, MD, USA, 2023. [CrossRef]
41. Gibson, N.D.; Walter, C.W.; Crocker, C.; Wang, J.; Nakayama, W.; Yukich, J.N.; Eliav, E.; Kaldor, U. Electron Affinity of Gallium and Fine Structure of Ga-: Experiment and Theory. *Phys. Rev. A* **2019**, *100*, 052512. [CrossRef]
42. Scheer, M.; Brodie, C.A.; Bilodeau, R.C.; Haugen, H.K. Laser Spectroscopic Measurements of Binding Energies and Fine-Structure Splittings of Co−, Ni−, Rh−, and Pd−. *Phys. Rev. A* **1998**, *58*, 2051. [CrossRef]
43. Gale, J.D.; Rohl, A.L. The General Utility Lattice Program (GULP). *Mol. Simul.* **2003**, *29*, 291–341. [CrossRef]
44. Plimpton, S. Fast Parallel Algorithms for Short-Range Molecular Dynamics. *J. Comput. Phys.* **1995**, *117*, 1–19. [CrossRef]
45. Zahn, D.; Schilling, B.; Kast, S.M. Enhancement of the Wolf Damped Coulomb Potential: Static, Dynamic, and Dielectric Properties of Liquid Water from Molecular Simulation. *J. Phys. Chem. B* **2002**, *106*, 10725–10732. [CrossRef]
46. Hill, R. The Elastic Behaviour of a Crystalline Aggregate. *Proc. Phys. Soc. Sect. A* **1952**, *65*, 349–354. [CrossRef]
47. Kovnir, K.; Schmidt, M.; Waurisch, C.; Armbrüster, M.; Prots, Y.; Grin, Y. Refínement of the Crystal Structure of Dipalladium Gallium, Pd_2Ga. *Z. Für Krist. -New Cryst. Struct.* **2008**, *223*, 7–8. [CrossRef]
48. Armbrüster, M.; Borrmann, H.; Wedel, M.; Prots, Y.; Giedigkeit, R.; Gille, P. Refinement of the Crystal Structure of Palladium Gallium (1:1), PdGa. *Z. Fur Krist. Cryst. Struct.* **2010**, *225*, 617–618. [CrossRef]
49. Krajčí, M.; Hafner, J. Semihydrogenation of Acetylene on the (010) Surface of $GaPd_2$: Ga Enrichment Improves Selectivity. *J. Phys. Chem. C* **2014**, *118*, 12285–12301. [CrossRef]
50. Taccardi, N.; Grabau, M.; Debuschewitz, J.; Distaso, M.; Brandl, M.; Hock, R.; Maier, F.; Papp, C.; Erhard, J.; Neiss, C.; et al. Gallium-Rich Pd-Ga Phases as Supported Liquid Metal Catalysts. *Nat. Chem.* **2017**, *9*, 862–867. [CrossRef]

Disclaimer/Publisher's Note: The statements, opinions and data contained in all publications are solely those of the individual author(s) and contributor(s) and not of MDPI and/or the editor(s). MDPI and/or the editor(s) disclaim responsibility for any injury to people or property resulting from any ideas, methods, instructions or products referred to in the content.